Dissociations and associations between shape and category representations in the two visual pathways

Stefania Bracci and Hans Op de Beeck
Laboratory of Biological Psychology, KU Leuven, 3000, Belgium

Corresponding author: stefania.bracci@kuleuven.be
Running Title: Shape and category in the two visual pathways

Summary
The dorsal and ventral visual pathways represent both visual and conceptual object properties. Recent reports suggested the role of low-level visual properties in driving the organization of high-level conceptual representations. However, these studies did not directly compare object shape and object category information. We present an event-related fMRI study with a two-factorial stimulus set with 54 images that explicitly dissociates shape from category in order to investigate their independent contribution as well as their interactions through representational similarity analyses. Results reveal a contribution from each dimension in both streams, with a transition from shape to category along the posterior-to-anterior anatomical axis. The nature of category representations differs in the two pathways: ventral areas represent object animacy and dorsal areas represent object action properties. Furthermore, information about shape evolved from low-level pixel-based to high-level perceived shape following a posterior-to-anterior gradient similar to the shape-to-category emergence. To conclude, results show that representations of shape and category independently coexist but at the same time they are closely related throughout the visual hierarchy.

Significant statement
Research investigating visual cortex conceptual category representations rarely takes into account visual properties of objects. In this report, we explicitly dissociate shape from category and investigate independent contributions and interactions of these two highly correlated dimensions.

Key words: visual cortex, object category, object shape, cortical organization, representational similarity analysis.

Introduction

Visual information is processed throughout a series of hierarchical stages in at least two pathways: a ventral stream for object recognition, and a dorsal stream for the visual guidance of actions (Goodale and Milner, 1992; Kravitz et al., 2013). At different stages along the ventral visual pathway, neurons are tuned to object contours and curvatures, position and three-dimensional object configurations (Kobatake and Tanaka, 1994; Brincat and Connor, 2004; Yamane et al., 2008). Higher up, in both human and monkey inferotemporal (IT) cortex, a large-scale division for animate and inanimate entities and further subdivisions within the animate domain for faces and bodies have been shown (Kiani et al., 2007; Kriegeskorte et al., 2008b; Bell et al., 2009). Although, a large body of evidence has shown that the ventral stream plays a critical role in representing both shape and semantic information (e.g., Grill-Spector et al., 1998), recently there has disagreement about the relative contribution of these two dimensions – and the nature of their interaction – in driving the visual cortex organization.

In particular, recent work in monkeys (Rajimehr et al., 2011; Baldassi et al., 2013; Yue et al., 2014) as well as in humans (Nasr et al., 2014; Rice et al., 2014; Watson et al., 2014) has argued that the organization of category representations in high-level visual cortex reflects brain selectivity for visual features, including relatively low-level dimensions such as spatial frequency and local orientation content which are typically associated with primary visual cortex. Similar unresolved discussions have arisen in the literature on the dorsal visual pathway (Sakuraba et al., 2012).

These controversies arise and are not easy to resolve because category distinctions are typically correlated with visual dimensions. Entities within the same object category share similar shape features. Faces are round and bodies are elongated. Most animals have four legs, a face and round contours that largely differ from most man-made inanimate objects (e.g., a bookshelf). Given these constraints, it is not surprising that most studies investigating category selectivity do not control for shape differences among stimuli within and across classes. Typically, such studies resort to the post-hoc application of relatively limited computational models to argue that category effects cannot be reduced to visual features. However, these visual features are never captured fully by the models (Kriegeskorte et al., 2008a; Op de Beeck et al., 2008b). Thus, it is hard to exclude the possibility that observed large-scale divisions (e.g., animate/inanimate) might be largely accounted for by object shape information.

To address these issues and compare the contribution of shape and category information within the two visual pathways, we implemented a two-factorial event-related fMRI design where shape and category membership are manipulated independently. This design allowed us to separate object shape and object category and investigate the contribution of the two factors.

Materials and Methods

Participants
The fMRI study included 15 right-handed adult volunteers (8 females; mean age, 24 years). One participant was excluded because of excessive head motion. All participants gave informed consent to take part in the fMRI experiment. The study was approved by the ethics committee of the KU Leuven.

Stimuli
The 54 stimuli are shown in Figure 1. Six categories of objects were included in an event-related design fMRI experiment: minerals, animals, fruit/vegetables, musical instruments, sport articles, and tools. Each category consisted of 9 greyscale images on a white background and had a size of 8° x 8° (400 x 400 pixels). For each category, each image had unique shape properties, thus creating 9 subsets of images with similar shape properties. Thus, the category and shape dimension were orthogonal to each other; each shape type (e.g., round) contained 1 image from each of the 6 object categories and each object category (e.g., animals) contained 1 image from each shape type. The nine summed images obtained by summing all images from each shape type are shown in the last row of Figure 1. The six summed images obtained by summing all images from each object category are shown in the last column of Figure 1. These six summed images suggest that object category could not be distinguished based on object shape properties. As a measure of image low-level shape properties (image silhouette), we computed pixelwise similarities among images (Op de Beeck et al., 2008b). For the silhouette model, the resulting dissimilarity matrix (1 minus correlation) is reported in Figure 2a (left most column). The value in each cell (upper triangle) of this dissimilarty matrix reflects pixel-based differences for each object pair (blue represents large similarity). For the silhouette model, the two-dimensional arrangement derived from multidimensional scaling (MDS) is reported Figure 2b.

Behavioral similarity judgments
Similarity judgments for the category and shape dimensions were rated by an independent group of participants (N=16) using the multiple object arrangement method (Kriegeskorte and Mur, 2012). Differently from pairwise similarity judgments, the multi-arrangement method allows for measuring multiple similarity judgments in a single arrangement, thus allowing each item to be rated in the context of all the remaining items (Kriegeskorte and Mur, 2012). Each participant rated all 54 images used in the functional neuroimaging study. For shape similarity, participants were asked to arrange the images based on perceived object shape similarity. For semantic category similarity, participants were asked to arrange the images based on the semantic similarity among objects. Results were averaged across participants. The shape and semantic category models are summarized in Figure 2 by means of dissimilarity matrices (Fig. 2a) and multidimensional scale arrangements (Fig. 2b).

Scanning procedure
The study consisted of two separated sessions, each performed in separated days. Each session included experimental runs as well as localizer runs. The stimuli presentation was controlled by a PC running the Psychophysics Toolbox package (Brainard, 1997) in MATLAB. Pictures were projected onto a screen and were viewed through a mirror mounted on the head coil.

Experimental runs: Each session included 8 experimental runs (16 in total), each lasting 7 minutes and 40 seconds each. Within each run a fully randomized sequence of 54 image trials (repeated 2 times) and 18 fixation trials (repeated 2 times) was presented. Each trial was presented for 1500 ms, followed by a fixation screen for 1500 ms. Each run started and ended with 14 seconds of fixation. Participants performed a 1-back real-world size judgment task by pressing a button with their right

index or middle finger if the current image was smaller or larger relative to the image presented in the previous trial. The fingers associated with each response were counterbalanced across runs.

Localizer runs: Seven categories of objects were included in a block-design fMRI localizer: whole bodies, hands, faces, tools, chairs, places, and scrambled images. Each condition consisted of 18 greyscale images (400 x 400 pixels) on a white background. In total, 4 functional localizer runs (2 runs for each session) were included in the study, each lasting 5 minutes and 12 seconds. Within each run a fully randomized sequence of 7 category blocks (each repeated 4 times) interleaved with a fixation block lasting 16 seconds was presented. At the beginning and at the end of each run an additional fixation block was presented for 14 seconds. Within each category block, images were presented at the center of the screen for 400 milliseconds with a blank interstimulus interval (ISI) of 400 milliseconds. Participants performed a 1-back repetition detection task by pressing a button with their right index finger any time the same picture was presented two times in succession. In each block, 1 or 2 repetitions were presented.

Imaging parameters

Data collection was performed on a 3T Philips scanner with a 32-channel coil at the Department of Radiology of the University Hospitals Leuven. MRI volumes were collected using echo planar (EPI) T2*-weighted scans. Acquisition parameters were as follows: repetition time (TR) of 2 s, echo time (TE) of 30 ms, flip angle (FA) of 90°, field of view (FoV) of 216 mm, and matrix size of 72 x 72. Each volume comprised 37 axial slices (covering the whole brain) with 3 mm thickness and no gap. The T1-weighted anatomical images were acquired with an MP-RAGE sequence, with 1 x 1 x 1 mm resolution.

Preprocessing and data analysis

Imaging data were preprocessed and analyzed using the Statistical Parametrical Mapping software package (SPM 8, Welcome Department of Cognitive Neurology, London, UK) and MATLAB. Functional images underwent the following preprocessing steps: slice timing correction, spatial realignment (to the first image) to adjust for individual head motion, co-registration of functional and anatomical images, segmentation and spatial normalization to an MNI (Montreal Neurological Institute) template. Functional images were resampled to a voxel size of 3x3x3 mm and spatially smoothed by convolution of a Gaussian kernel of 4 mm full-width at half-maximum (Op de Beeck, 2010).

We modelled the pre-processed signal for each voxel, for each participant and for each of the 54 images using a general linear model (GLM). The GLM included regressors for each condition of interest (54 conditions) and the 6 motion correction parameters (x, y, z for translation and for rotation). Each predictor's time course was modelled by a boxcar function convolved with the canonical hemodynamic response function in SPM.

Regions of interest

Fifteen regions of interest (ROIs), which covered the wider lateral and ventral surface of OTC (LOTC; VOTC), and part of parietal and frontal cortices, were defined in each individual participant. ROIs were defined by means of an independent functional localizer and (when necessary) the anatomical WFU PickAtlas Toolbox (Wake Forrest University PickAtlas, http://fmri.wfubmc.edu/cms/software). Object-selective voxels (chairs > scrambled images) were localized in lateral and ventral occipital temporal cortex (Grill-Spector and Malach, 2004). Face-selective voxels [conjunction of (faces > chairs) and (faces > bodies)] and body-selective voxels (bodies > chairs) could be defined separately in LOTC (LOTC-face, LOTC-body; Puce et al., 1996; Downing et al., 2001) but not in VOTC (Peelen and Downing, 2005; Schwarzlose et al., 2005), where face and body voxels (face + body > chairs) were combined in a single ROI (VOTC-face/body). Hand-selective voxels [conjunction of (hands > chairs) and (hands > bodies)] were defined in LOTC (LOTC-hand; Bracci et al., 2010). Additional hand-selective voxels (hands > chairs) were defined in the intraparietal sulcus (IPS-hand). Scene-selective

voxels (scenes > chairs) were defined in the transverse occipital sulcus (TOS-scene; Nasr et al., 2011), posterior and anterior parahippocampal gyrus (pPPA-scene, aPPA-scene; Arcaro et al., 2009). Early visual areas (EVC-1 and EVC-2; all categories > baseline) were restricted to anatomical masking by Brodmann areas, BA-17 and BA-18 respectively. Superior parietal lobe (SPL; all categories > baseline) and inferior parietal lobe (IPL; all categories > baseline) were restricted to the anatomical mask BA-5/7 and BA-40, respectively. Finally, dorsal prefrontal cortex (DPFC; all categories > baseline) was restricted to the anatomical mask BA-46. ROIs included all spatially contiguous voxels that exceeded the statistical uncorrected threshold $p < 0.001$. When less than 25 active voxels were found at this threshold, a more liberal threshold of $p < 0.01$ was applied. Only ROIs with at least 25 active voxels were included in an individual subject. To ensure that all ROIs were anatomically independent from each other a hierarchical inclusion criterion was applied which reflected the functional criterion. For example, if a subset of object-selective voxels were also selective for bodies, object-selective voxels were defined after excluding body-selective voxels (those voxels where the response to bodies was significantly higher than chairs). Table 1 reports details on ROIs' localization (e.g., functional contrast, cluster size) and Figure 3 shows all ROIs in one representative participant. These ROIs provide a continuous and comprehensive window on the large cortical area activated when perceiving objects, the latter being displayed in grey on the small brain maps in Figure 3 (all categories > baseline, p = 0.00001, uncorrected). With the exception of the region around the central sulcus, which is probably activated due to the execution of the motor response, a large part of the regions activated by viewing the object images is covered by the aforementioned ROIs. The choice of combining functional and anatomical criteria to define our ROIs – over possible alternatives such as anatomical parcellation – was preferred. This combined method (in several variations), very common in research on the visual system, allows determining functionally specific ROIs by including a large portion of visually active voxels and at the same time excluding voxels that do not show reliable visually object-related information.

Note that the ROIs differed in size. Whereas differences in ROIs size can lead to differential results in classification-based analyses, correlation-based analyses are not affected by different ROI's size. To confirm this, we repeated our analyses using the same number of voxels for each ROI. As expected, exactly the same results were obtained in the two analyses.

Multivoxel pattern analysis

We used correlation-based multivoxel pattern analysis to analyse how the spatial response pattern in individual ROIs differs between experimental conditions (Haxby et al., 2001). Parameter estimates ('responses') for each condition (relative to baseline) were extracted for each voxel in an ROI, for each participant and each run, and normalized per run by subtracting the mean response across all conditions for each voxel separately. The full dataset was divided into two independent subsets of runs (set-1 and set-2). The multi-voxel patterns of activity associated with each condition (e.g., fish) in set-1 were correlated with the activity patterns in set-2. This procedure of splitting the data in two was repeated 100 times. Correlations were averaged across the 100 iterations, thus resulting in an asymmetric 54 x 54 correlation matrix for each participant and ROI. Subsequently, the two halves (above and below the diagonal) of the correlation matrix were averaged and only the upper triangle of the resulting symmetric matrix was used in the following analyses. To test whether the response pattern in an ROI conveyed information about stimulus identity, we compared the average of within-condition correlations (diagonal cells) for each ROI with the average of between-condition correlations (off diagonal cells). Pairwise t-tests across participants revealed significant reliability of response patterns for each ROI ($p < 0.01$; for all tests). Thus, the multi-voxel patterns convey information about the presented conditions in all the ROIs. Subsequently, correlation matrices were converted into dissimilarities matrices (1 minus correlation) and used as neural input for the RSA analysis (Kriegeskorte et al., 2008a). As before (Op de Beeck et al., 2008b), we correlated the behavioural dissimilarity matrices for shape and semantic category with the neural dissimilarity matrix of each ROI. Resulting correlations were Fisher transformed {0.5*log[(1+r)/(1-r)]}.

To take into account the noise in the data, for each ROI we computed an estimate of the reliability of the data, which provides an indication of the maximum correlations we can expect given the signal to noise ratio of the data (Op de Beeck et al., 2008b). For each subject and each ROI, the 54 x 54 correlation matrix was correlated with the averaged correlation matrix of the remaining participants. Values were averaged across participants. The resulting correlation values capture noise inherent to a single subject as well as noise caused by inter-subject variability. This measure of reliability gives an estimate of the highest correlation we can expect in each ROI when correlating behavioural dissimilarity (e.g., shape model) and neural dissimilarity (e.g., activation pattern in each ROI). We provide this measure as a reference in all the relevant data figures (grey-shaded background bars). It would also be possible to normalize for reliability by dividing all correlations through the reliability, and such approach results in very similar statistics and conclusions as our main, not normalized analyses.

Multidimensional scaling and hierarchical cluster analysis.
Multidimensional scaling (MDS) and hierarchical cluster analysis were used to visualize and compare neural similarity structures in all ROIs and similarity structures related to pixel-based overlap (silhouette similarity) and the behavioural models (shape similarity and category similarity). Metric multidimensional scaling was performed using Matlab function “mdscale” normalized with the sum of squares of the dissimilarities. The hierarchical cluster analysis was performed using the Matlab function “linkage” using the nearest distance default method.

Results

Shape and category information in the ventral and dorsal pathway

We collected behavioural and neural data on a set of 54 images (Fig. 1). An independent group of participants (N =16) performed similarity judgments on all images for the shape and the semantic category dimension (Materials and Methods). As intended, the two dimensions were independent (r= -0.01), and revealed a very different representational space (Fig. 2b). To investigate how information about shape and category is distributed throughout the ventral and dorsal pathway, dissimilarity matrices derived from behavioural judgments (Fig. 2) were compared with neural dissimilarity matrices derived from regions of interests' (ROIs) activity patterns (Materials and Methods) by means of representational similarity analysis (RSA; Kriegeskorte et al., 2008a). Defined ROIs (Materials and Methods) covered a large cortical area of visually active voxels within both visual pathways (Fig. 3). As shown in Figure 4a, the neural similarity in most ROIs (BA-17, BA-18, TOS-scene, pPPA-scene, aPPA-scene, LOTC-object, LOTC-face, LOTC-body, LOTC-hand, VOTC-object, VOTC-body/face and SPL) showed significant above baseline correspondence with shape similarity as rated behaviourally ($p > 0.004$ for all tests; Fig. 4a marked with green asterisks). We refer to these regions as shape-*sensitive* ROIs. Shape information was not present in IPS-hand, IPL and DPFC. Different results were observed for the category dimension. Whereas category information was not present in early visual areas (EVC-1, EVC-2: $t < 1$ for both tests) and scene-selective areas (TOS, pPPA, aPPA: $t < 1$ for all tests), significant above baseline category information was observed in object/face/body/hand selective areas in lateral and ventral OTC (LOTC-object, LOTC-face, LOTC-body, LOTC-hand, VOTC-object, VOTC-body/face), SPL, IPL, IPS-hand and DPFC ($p < 0.01$ for all tests; Fig. 4a marked with orange asterisks). We refer to these regions as category-*sensitive* ROIs. Thus, category-related information is present even when shape similarity is orthogonal to category membership and goes against it so that stimuli with high shape similarity belong to different categories.

Next, we assessed how the representational content is changing across ROIs. To compare representational content across ROIs, we performed second-order correlations across ROI's correlation matrices averaged across subjects. The resulting dissimilarity matrix (1 minus correlation; Fig. 4b) captures similarities in representational content among ROIs: similarities in two ROIs' representational content (e.g., BA17 and BA18) suggest that these ROIs represent the stimuli in a similar manner. The application of multidimensional scaling to this ROI similarity matrix revealed a two dimensional arrangement (Fig. 4c) in which the first (horizontal) dimension seems related to the anatomical posterior-to-anterior axis, and the second dimension to the ventral-to-dorsal axis. In Figure 4c, the color-coding of the ROIs in terms of their selectivity for shape (green color-coded), category (orange color-coded) or both types of information (yellow color-coded) suggests a transition in representational content from shape-sensitive ROIs to category-sensitive ROIs along the anatomical posterior-to-anterior axis. To quantify the relationship between the type of selectivity and the anatomical position of an ROI, we correlated the ROI's mean anatomical location on the y-axis with the amount of category/shape information present in each ROI (cs-index = (category – shape)/(category + shape)). Further confirming results shown in Figure 4c, we found a highly positive correlation between ROI's mean anatomical location on the y-axis and the cs-index (r=0.76); from posterior to anterior, shape information decreases and category information emerges. Taken together, these results show a transition from object shape to object category along the posterior-to-anterior anatomical axis, with many regions in high-level visual cortex encoding both types of information.

In sum, we observed that category selectivity could not be reduced to object visual properties such as perceived shape. Nevertheless, many of the high-level visual regions encoded both dimensions of object images: the shape and the category they belong to. In the next sections, we will further characterize information content for shape-sensitive and category-sensitive ROIs separately.

Characterizing information content in category-sensitive ROIs

What type of "category" information is represented in category-sensitive ROIs? The hierarchical cluster analysis (Material and Methods) performed on category-sensitive ROIs (marked with orange asterisks in Fig. 4a) revealed two main clusters reflecting differences in ROIs' representational content (Fig. 5a): one cluster for more ventral ROIs in occipitotemporal cortex (light blue color-coded: LOTC-object, LOTC-body, VOTC-object, VOTCface/body, LOTC-face, LOTC-hand) and one cluster for more dorsal ROIs in parietal and prefrontal areas (dark blue color-coded: IPS-hand, SPL, DPFC, IPL). This clustering suggests differential category-related information content for areas within the dorsal and ventral visual pathway. Figure 5d shows the category clusters for one representative subject on a brain template.

The candidate hypotheses for the nature of these differences can be found in the literature. Although our results add to the increasing evidence that object representations are encoded in both visual pathways (Konen and Kastner, 2008; Grill-Spector and Weiner, 2014), the two streams are supposed to support different computations; whereas the ventral stream processing primarily supports object perception, such as the animate/inanimate division (Caramazza and Shelton, 1998), the dorsal stream processing sustains action-related computations (Buxbaum et al., 2014). Does information content in the ventral and dorsal cluster reflect this distinction? Up to now no single study directly compared these two hypotheses in ventral as well as dorsal visual cortex.

To address this question, we used RSA to compare neural similarity matrices derived from ROIs' activity patterns (averaged across ROIs within each cluster) to two category models: (1) The animate/inanimate model (Fig. 5b, light blue border) captures the animate/inanimate division previously reported in visual cortex (Kriegeskorte et al., 2008b; Konkle and Caramazza, 2013). This model assumes high correspondence between neural patterns for two animate objects (two animals) and for two inanimate objects (e.g., a mineral and a musical instrument), but low correspondence between neural patterns for one animate and one inanimate object (e.g., an animal and a mineral). (2) The action/non-action model (Fig. 5b, dark blue border) captures sensitivity to action-related properties of objects, which might be more emphasized in dorsal stream areas. Our stimulus set includes three action-related object categories (sport articles, musical instruments and tools). The action/non-action model predicts high correspondence between neural patterns for two action-related objects (e.g., a musical instrument and a tool) and two non-action objects (e.g., an animal and a mineral), but low correspondence between neural patterns for one action-related and one non-action object (e.g., a musical instrument and a mineral).

Results from RSA were tested in a 2 x 2 ANOVA with Cluster (ventral, dorsal) and Model (animate/inanimate, action/non-action) as within-subject factors. Results revealed a significant Cluster x Model interaction ($F_{(1,13)} = 31.15$, $p = 0.00009$; Fig. 5b), as such indicating that the differences in the relation between models and representational content in the ventral and dorsal cluster can be captured by these two models. Post-hoc pairwise t-tests further confirmed this dissociation: whereas in the ventral cluster (cluster 1) the animate/inanimate model could significantly better explain the neural pattern relative to the action/non-action model ($t_{13} = 4.70$, $p = 0.0004$; Fig. 5b), in the dorsal cluster (cluster 2) the action/non-action model was significantly more related to the neural data relative to the animate/inanimate model ($t_{13} = 2.9$, $p = 0.01$; Fig. 5b).

The correlations between the best model and the neural similarity matrix are not as high as they could be given the reliability of the data, thus representations in the ventral and the dorsal stream are not captured fully by any of these models. Nevertheless, the models capture important aspects of those representations. This is visible in the two-dimensional space formed by the dimensions that capture most variation in the neural similarity matrices according to multidimensional scaling. These spatial configurations illustrate the animate/inanimate (left panel) and the action/non-action (right panel) division in the ventral and the dorsal cluster, respectively (Fig. 5c). Thus, despite the fact that both ventral and dorsal regions show category information, this first direct comparison of the two pathways through RSA confirms that the informational content in ventral and dorsal regions differs and reflects the hypothesized different computations happening in the ventral and dorsal pathway.

Characterizing information content in shape-sensitive ROIs

What type of "shape" information is represented in shape-sensitive ROIs? The hierarchical cluster analysis (Materials and Methods) performed on shape-sensitive ROIs (marked with green asterisks in Fig. 4a) revealed two main clusters (Fig. 6a). Cluster 1 included BA-17, BA18, TOS-scene, pPPA-scene, LOTC-face and LOTC-object. Cluster 2 included VOTC-face/body, VOTC-object, LOTC-body and LOTC-hand. Two additional ROIs (SPL, aPPA-scene) did not group with either cluster, and were excluded from subsequent analyses. The ROIs in the two shape clusters differed in their anatomical location; along the posterior-to-anterior anatomical y-axis, single-subject MNI coordinates, averaged across ROIs within each cluster, were significantly more posterior in cluster 1 than in cluster 2 ($t_{11} = 22.2$, $p < 0.0001$; only subjects where all ROIs could be defined were included in this analysis). Figure 6d shows the shape clusters for one representative subject on a brain template. Taken together, these results suggest differential shape-related information content in posterior (cluster 1) and anterior (cluster 2) shape-sensitive ROIs.

In the visual system, information about shape is processed throughout a series of hierarchical stages, so that early visual areas process image low-level visual properties such as position and orientation (Hubel, 1963) and extrastriate visual areas represent perceived object shape (Haushofer et al., 2008; Op de Beeck et al., 2008b) in a way that is tolerant to changes in object position, size and orientation (Grill-Spector et al., 1999; James et al., 2002). To test whether representational content in the posterior and anterior "shape" cluster reflects this known hierarchical shape processing, we used RSA to compare neural similarity matrices derived from ROIs' activity patterns (averaged across ROIs within each cluster) to two shape models: (1) the "low-level" shape model (silhouette model), based on image pixel-wise similarities, and (2) the "high-level" shape model (shape similarity), derived from shape similarity judgments, which is the shape model used up to now in the Results section. Figure 2b and 6b illustrate the two models and their differences. The two shape models correlate only partially ($r = 0.25$). Clear differences between the two models are obvious from visual inspection of the multidimensional scaling solutions (Fig. 2b): in the perceived shape model, shape types cluster in three main subdivisions (i.e., elongated shapes (different shades of red), round shapes (different shades of green) and triangular shapes (different shades of blue)). These divisions are not present in the silhouette model were the three elongated shape types are largely segregated. Stated otherwise, the judged shape similarity shows more tolerance for the image orientation of elongated stimuli.

Results from the RSA were tested in a 2 x 2 ANOVA with Cluster (posterior, anterior) and Model (silhouette, shape) as within-subject factors. This analysis revealed a significant Cluster x Model interaction ($F_{(1,13)} = 11.6$, $p = 0.005$; see Fig. 6b), as such confirming differences in the relation between models and representational content in the posterior and anterior shape-sensitive ROIs. Post-hoc pairwise t-tests further confirmed this difference: whereas in the posterior cluster (cluster 1) the silhouette model could significantly better explain the neural pattern relative to the shape model ($t_{13} = 2.20$, $p = 0.05$; Fig. 6b), in the anterior cluster (cluster 2) the shape model was significantly more related to the neural data relative to the silhouette model ($t_{13} = 4.71$, $p = 0.0004$; Fig. 6b). There was also a main effect of Cluster ($F_{(1,13)} = 90.5$, $p < 0.0001$), with much higher correlations overall in cluster 1 than in cluster 2. This main effect is at least in part a trivial consequence of the differences in reliability of the multi-voxel patterns in the two clusters (grey bars in Fig. 6b). We should also note that the fit with the best shape model is far from perfect in each cluster: the highly significant correlations between the best model and the neural similarity data are smaller than what could be expected given the reliability of the data.

In Figure 6c, the two-dimensional arrangements derived from multidimensional scaling illustrate the representational structure in the posterior (left panel) and anterior (right panel) "shape" cluster. Consistent with the models, in the posterior cluster, vertical elongated objects (red color-coded stimuli) and horizontal elongated objects (dark red color-coded stimuli) were largely dissociated, whereas all elongated objects clustered together in the anterior cluster.

Relation between the representation of shape and category

The orthogonal manipulation of shape and category has allowed us to assess the separate contribution of each factor. In addition we can investigate potential relations between the two factors. Despite the relatively artificial dissociation in our stimulus set, in a more general context shape can be a reliable cue to recognize, identify, and categorize an object. Not just any shape feature is useful though, and in the literature it has been suggested that a shape representation useful for object recognition and basic-level categorization should be sensitive to features that allow transformation-invariant object recognition (Biederman, 1987; Kayaert et al., 2003). The above results showed that we have the sensitivity in our dataset to differentiate between low-level pixel-based shape features and more high-level shape representations: along the visual pathway, from posterior to anterior, there is a progression from "low-level" to "high-level" shape representation. If this subjective shape perception (e.g., recognizing elongate shapes irrespective of orientation) has any role in the ability to categorize objects at a superordinate level (e.g., animate versus inanimate), then we expect a close relationship between subjective perception of shape and semantic category sensitivity across the ROIs sensitive to shape (all ROIs marked in green in Fig. 4a).

To investigate this question, we analyzed all ROIs with significant shape sensitivity (BA-17, BA-18, TOS-scene, pPPA-scene, aPPA-scene, LOTC-object, LOTC-face, LOTC-body, LOTC-hand, VOTC-object, VOTC-body/face and the SPL). We calculated the relative amount of high-level as compared to low-level shape information, referred to as the *perceived shape* index (ps-index) by subtracting the correlation with the "low-level" shape silhouette model (shown in light blue in Fig. 6b) from the correlation with the "high-level" perceived shape model (shown in dark blue in Fig. 6b) separately for each shape-sensitive ROI. Results for the ps-index and for category similarity (as reported in Fig. 4a, orange color-coded) are shown for all shape-sensitive ROIs in Figure 7a. The correlation between the ps-index and category information (averaged across subjects) was highly significant across the 12 ROIs ($r_{(10)} = 0.74$, $p = 0.006$), thus suggesting a close relationship between hierarchical shape processing and category selectivity in visual areas (Fig. 7b). This statistical analysis only takes into account the variation across ROIs to determine significance. The same analysis performed on single subjects, confirmed that the relation between the ps-index and category information across shape-sensitive ROIs is significantly positive when considering the variation across subjects (one sample t-test computed across individual subject's correlation values: $t_{11} = 17.24$, $p = 0.0001$; only subjects where all ROIs could be defined were included in this analysis). In sum, even though we have shown that semantic category selectivity cannot be reduced to shape selectivity, nor vice versa, we observed a close association between the two dimensions so that shape representations include more high-level shape properties in more category sensitive regions.

Discussion

In addition to shared functional/semantic properties, objects within the same category typically share similar visual features. Here we created a stimulus set where the category and the shape dimension were orthogonal to each other, thus allowing disentangling their unique contribution to object representations. We found evidence for: (i) category representations with different properties in the ventral and the dorsal stream, (ii) shape representations of varying complexity, and (iii) association between category and shape representations.

First, the pattern of activity in many regions in lateral and ventral occipitotemporal cortex was related to the category membership of stimuli. As such, our results put into perspective recent findings suggesting that the organization of category representations in the ventral visual pathway can be, in large part, reduced to relatively simple visual properties (Rice et al., 2014; Watson et al., 2014). Nevertheless, the ventral category-sensitive regions, often regarded as the highest stage in visual information processing, also show shape sensitivity in addition to category sensitivity. As such the present study allows us to conclude that lateral and ventral occipitotemporal representations contain information about category as well as shape. Thus, extreme suggestions that one of the two dimensions can be explained by the other dimension are contradicted by the current results. Studies like ours are needed to determine the relative weight given to these dimensions.

There are of course other visual properties beyond shape. Nevertheless, shape is a very prominent alternative explanation for apparent category selectivity (Baldassi et al., 2013; Rice et al., 2014; Watson et al., 2014). Importantly, our manipulation of overall shape also introduces large variations in other properties, making it unlikely that any other visual property could explain the consistent category selectivity. Thus, category selectivity is remarkably tolerant to large variations in shape and other visual properties.

These results revealed that both visual streams encode information about object category. However, dorsal and ventral representations differed significantly in terms of their category information content. Regions in the ventral visual pathway mostly represent the animate/inanimate division. This result confirms the conclusion of previous studies (Kriegeskorte et al., 2008b), now with a stimulus set that dissociates this category distinction from other visual properties, and even without including exemplars from two very prominent classes of animate stimuli: human faces and bodies. Conversely, dorsal stream areas represent whether an object, regardless of its shape properties, is functionally associated with an action (musical instruments, sport articles, tools) or not (minerals, animals, fruit/vegetables). This is consistent with the proposed role of object representations in the dorsal stream. Neuropsychological studies have shown that whereas lesions in the ventral stream drastically affect object recognition (Caramazza and Shelton, 1998), parietal lobe lesions impair hand-object interactions, such as the ability to manipulate objects according to their function (Buxbaum et al., 2014). This evidence, together with functional neuroimaging studies showing, in parietal areas, selectivity for tools but not to other graspable objects (Chao and Martin, 2000; Valyear et al., 2007), suggest that object representations within the dorsal pathway might encode object functional and motor representations necessary to perform skilful actions.

As a second point, our results illustrate the distribution and transformations in how shape is represented. Shape representations were remarkably widespread throughout the ventral visual pathway, including more anterior occipitotemporal regions, where shape and category information co-existed. Within the shape domain, we observed a progression of shape representations from early visual areas to high-level visual areas; whereas representational content in more posterior areas (e.g., BA 17/18) was best predicted by the silhouette model, higher up in high-level visual areas, representations reflected perceived shape similarities (Fig. 6). The properties of high-level shape representations were in line with earlier reports (Eger et al., 2008) showing an increased degree of orientation invariance (all elongated objects cluster together despite differences in orientation). These results confirm evidence from multivariate analyses obtained earlier with artificial objects (Haushofer et al., 2008; Op de Beeck et al., 2008b), and show that these earlier conclusions hold for

images of real, everyday objects. Perceived shape similarity of familiar categories is represented in many category-selective regions.

As a third point, our results suggest a relationship between shape and category representations. The degree to which information content in shape-sensitive ROIs reflected perceived rather than low-level shape properties was closely related to the degree to which that same ROI encoded category information (Fig. 7). These results suggest that object shape representations in high-level visual cortex might be influenced by the interaction with object semantic knowledge, or vice versa. This perspective differs from the point of view taken in most existing literature. Many studies have argued in favour of one dimension, category selectivity (Kanwisher, 2010) or particular visual properties (Ishai et al., 1999). Our findings indicate that either dimension cannot be explained by the other. Furthermore, these dimensions show interesting associations that might inform on why many properties co-exist. Op de Beeck and colleagues (2008a) already suggested that category selectivity might be based upon the coincidence of multiple features, each of which might be correlated to some degree with category distinctions. Many of such feature maps have been demonstrated, including eccentricity biases (Levy et al., 2001; Hasson et al., 2002), curvature/shape (Brincat and Connor, 2004; Yamane et al., 2008) and spatial frequency (Rajimehr et al., 2011). Nevertheless, category selectivity cannot be reduced to a simple linear combination of these features. As the current study shows, category selectivity is robust even when the other features are not consistently associated with category membership or even manipulated independently from category membership. Instead, as suggested by the found association between perceived shape sensitivity and category sensitivity, it might be worthwhile to reverse our viewpoint and question to what extent can we understand the existing feature maps by assessing their usefulness for categorizing objects.

Indeed, the observed feature maps and their relationships are difficult to understand without taking into account the relationship to category representations. As far as our results are concerned, the goal of recognizing and categorizing objects might be an important factor to understand the transition from low-level to high-level shape representations. As another example, the bias of face-selective regions to prefer curved objects, lower spatial frequencies, and foveally presented stimuli is hard to explain without resorting to the concept of a face (Op de Beeck et al., 2008a). In early visual cortex, neurons that prefer foveal stimuli typically process higher spatial frequencies, not lower spatial frequencies. Thus, why would one and the same region prefer lower spatial frequencies and foveally presented stimuli if not for the fact that face recognition typically involves the processing of lower spatial frequencies of foveated faces? Thus, to understand how and why the functional organization for such visual properties is correlated with category selectivity, we might have to consider the association of these properties with category information throughout everyday visual experience.

To conclude, our results provide a significant advance in the debate of to what extent object shape and object category underlie the functional organization of object representations in visual cortex. We created a stimulus set that allowed disentangling the shape and the category dimension. Notably, our results show that object category representations in both visual pathways cannot be reduced to object shape properties. At the same time, shape and category information interact throughout the visual hierarchy shaping object perception in a fundamental way, ultimately leading to successful object recognition.

Figures and Tables Legends

Figure 1. Experimental stimuli. The stimulus set consisted of 54 unique images comprising 6 object categories (rows) and 9 shape types (columns). Each object category (e.g., minerals) included 9 images (one from each shape type), with unique shape features. Each shape type included 6 images (one from each object category) with similar shape features. The pixelwise overlap obtained by summing all images from each shape type and each object category are shown in the last row and last column respectively. Analyses of the 54x54 dissimilarity matrix (Fig. 2a-b, left most column) obtained from the pixel-based overlap between pairs of images reveal how strongly this physical measure of low-level dissimilarity is dominated by shape: large differences between stimuli from the same object category, and small differences between stimuli from the same shape type (Fig. 1, last row and last column). Thus, object category could not be distinguished based on shape information.

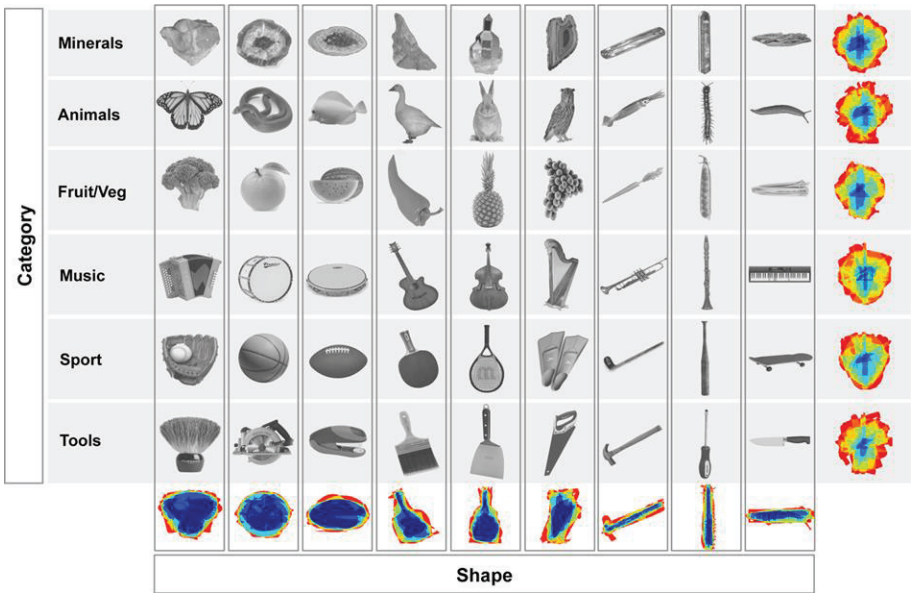

Figure 2. Models. (A) Mean representational dissimilarity matrices (red color indicates large dissimilarities), and (B) two-dimensional arrangements derived from multidimensional scaling for the silhouette model (left most panel), the perceived shape model (middle panel) and the category model (right most panel). Correlations between dissimilarity matrices are as follow: silhouette similarity and shape similarity (r = 0.25); silhouette similarity and category similarity (r = -0.05); shape similarity and category similarity (r = -0.01).

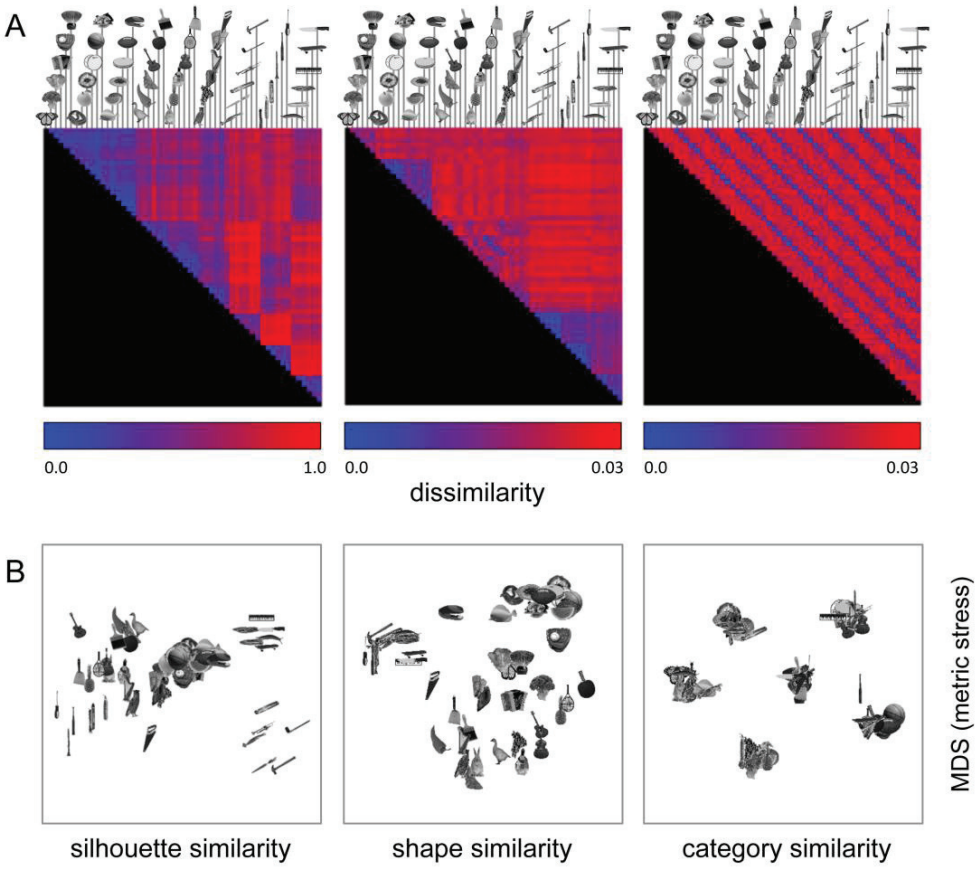

Figure 3. Regions of interest. Individual-participant ROIs are shown for the left hemisphere of one representative participant on a ventral, lateral and posterior view of the inflated PALS human brain template (Van Essen, 2005). Small brain maps display the significantly activated voxels when contrasting all categories included in the localizer with the fixation baseline (p = 0.00001, uncorrected). LH, left hemisphere.

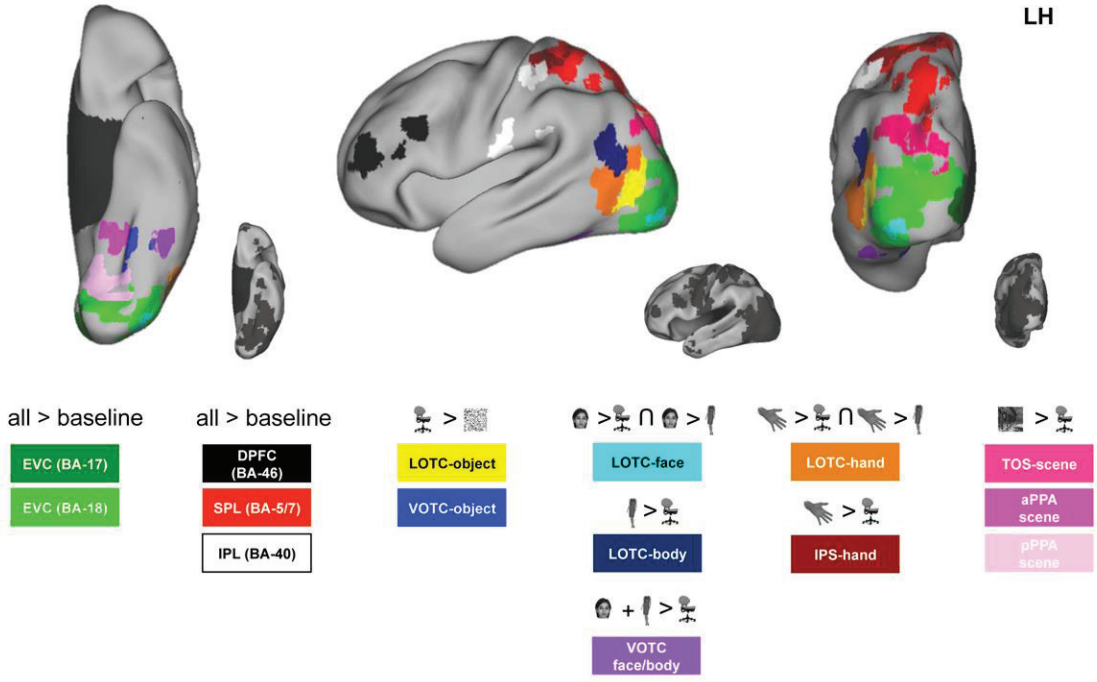

Figure 4. Representational similarity analysis for shape and category. (A) Results of region of interest RSA for the shape similarity (green color-coded) and the category similarity (orange color-coded). Green and orange asterisks highlight ROIs with significant shape and category information, respectively. For each ROI, the grey-shaded background bar represents the reliability of the correlational patterns in each ROI, which provides an approximate upper bound of the observable correlations between behavioural and neural data. (B) The dissimilarity matrix derived from second-order correlations across ROI's correlation matrices (averaged across subjects), shows similarities across ROI's representational content. Blue represents similar ROI's structural content. (C) Multidimensional scaling, performed on the ROI dissimilarity matrix from panel B, shows ROIs pairwise distances in a two dimensional arrangement. Pairwise distances reflect response-pattern similarity: ROIs positioned next to each other have a similar information content, whereas ROIs positioned far from each other show dissimilar information content. (D) Shape-sensitive (green color-coded), category-sensitive (orange color-coded) and both shape/category-sensitive (yellow color-coded) ROIs are shown for one representative subject on the inflated PALS human brain template (Van Essen, 2005). LH, left hemisphere.

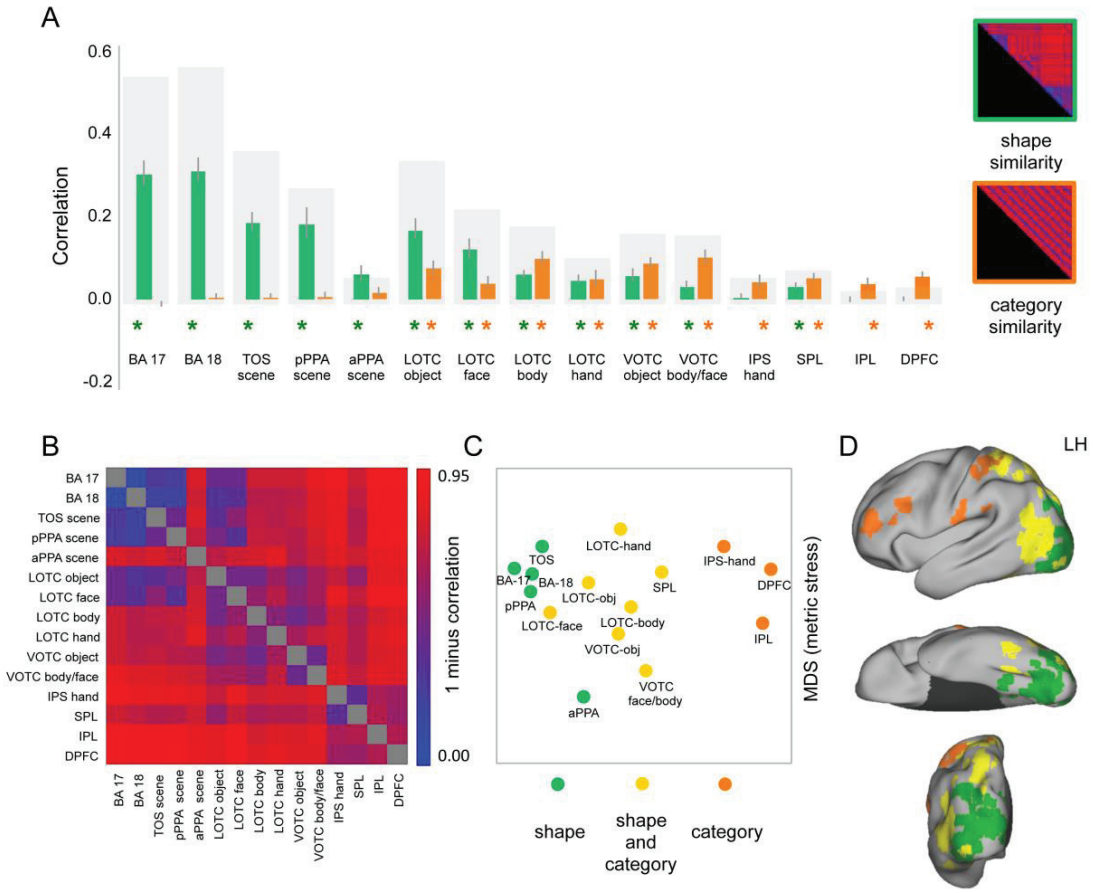

Figure 5. Characterizing information content in category-sensitive ROIs. (A) The hierarchical plot derived from a hierarchical cluster analysis shows ROI's activity-pattern similarity structure for category-sensitive ROIs. Results revealed two separated clusters: one (cluster 1) for ventral stream areas, and one (cluster 2) for dorsal stream areas. (B) Results of RSA at the cluster level for the animate/inanimate model (light blue color-coded) and the action/non-action model (dark blue color-coded). For each cluster, the grey-shaded background bar represents the reliability of the correlational patterns in each cluster. (C) Multidimensional scaling, performed on neural dissimilarity matrices (1 minus correlation), averaged across ROIs within each cluster, shows objects pairwise distances in a two-dimensional space for the ventral cluster (left panel) and the dorsal cluster (right panel). Pairwise distances reflect response-pattern similarity: the animate/inanimate division and the action/non-action division are clearly visible in the ventral cluster (left panel) and the dorsal cluster (right panel), respectively. (D) ROIs from cluster 1 (light blue color-coded) and cluster 2 (dark blue color-coded) are shown for one representative subject on the inflated PALS human brain template (Van Essen, 2005). LH, left hemisphere.

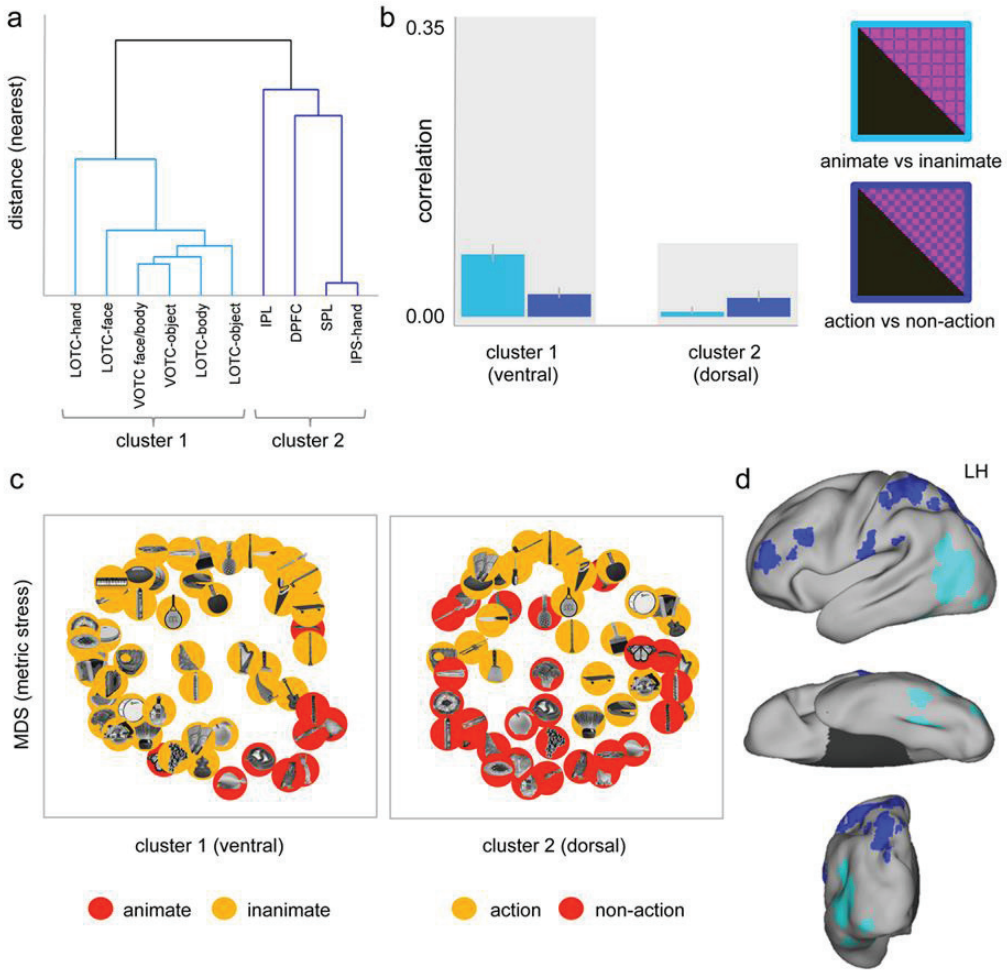

Figure 6. Characterizing information content in shape-sensitive ROIs. (A) The hierarchical plot derived from the hierarchical cluster analysis shows ROI's activity-pattern similarity structure for shape-sensitive ROIs. Results revealed two separated clusters: cluster 1 (BA-17, BA-18, pPPA-scene, TOS-scene, LOTC-face, LOTC-object) and cluster 2 (LOTC-body, VOTC-object, VOTC-face/body, LOTC-hand). (B) Results of RSA at the cluster level for the silhouette model (light blue color-coded) and the perceived shape model (dark blue color-coded). For each cluster, the grey-shaded background bar represents the reliability of the correlational patterns in each cluster. (C) Multidimensional scaling, performed on neural dissimilarity (1 minus correlation) matrices averaged across ROIs within each cluster, shows objects pairwise distances in a two dimensional space for the posterior cluster (left panel) and the anterior cluster (right panel). Pairwise distances reflect response-pattern similarity. (D) ROIs from cluster 1 (light blue color-coded) and cluster 2 (dark blue color-coded) are shown for one representative subject on the inflated PALS human brain template (Van Essen, 2005). LH, left hemisphere.

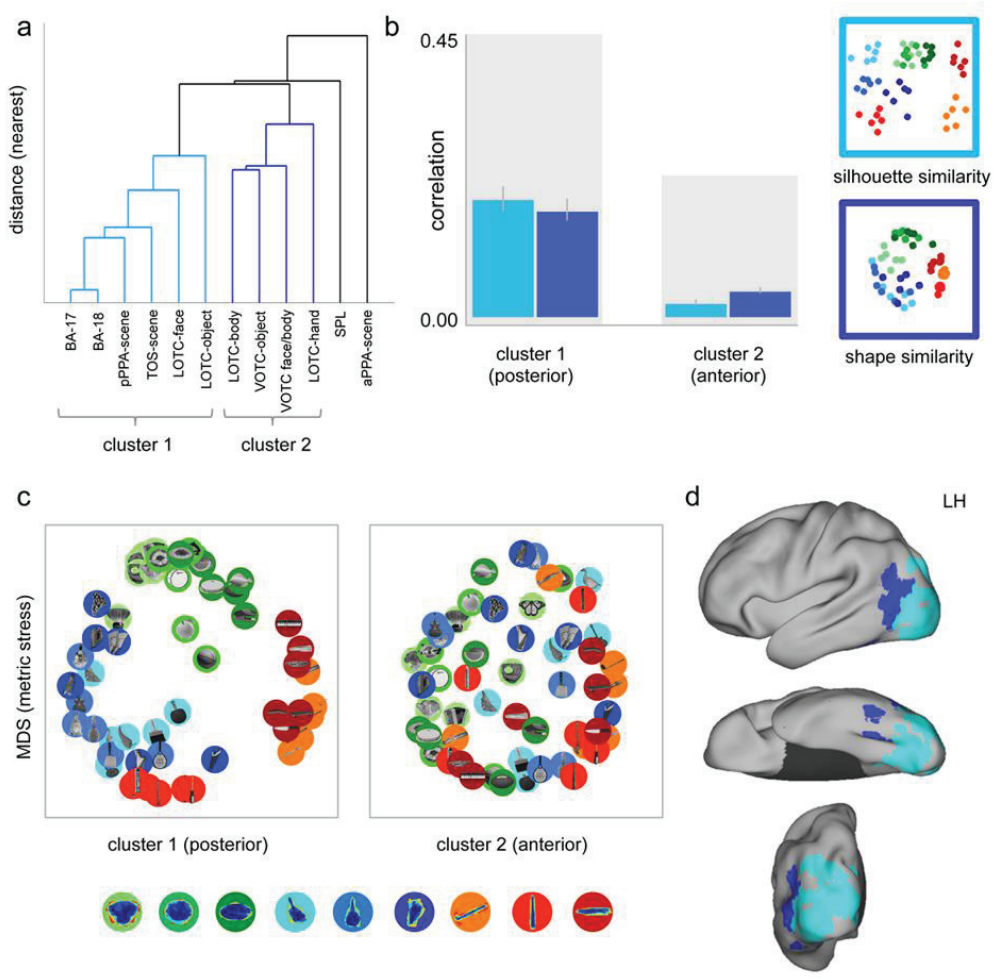

Figure 7. Interaction between shape and category. (A) Results of region of interest RSA for the perceived shape (ps-)index (light blue color-coded) and the category similarity (dark blue color-coded) in shape-sensitive ROIs. The ps-index reflects the relative amount of high-level as compared to low-level shape information and was computed by subtracting "low-level" shape silhouette information (shown in light blue in Fig. 6b) from "high-level" perceived shape information (shown in dark blue in Fig. 6b) separately for each shape-sensitive ROI. For each ROI, the grey-shaded background bar represents the reliability of the correlational patterns in each ROI. (B) Scatterplot of the relationship between the ps-index and category information (averaged across subjects) across the 12 shape-responding ROIs.

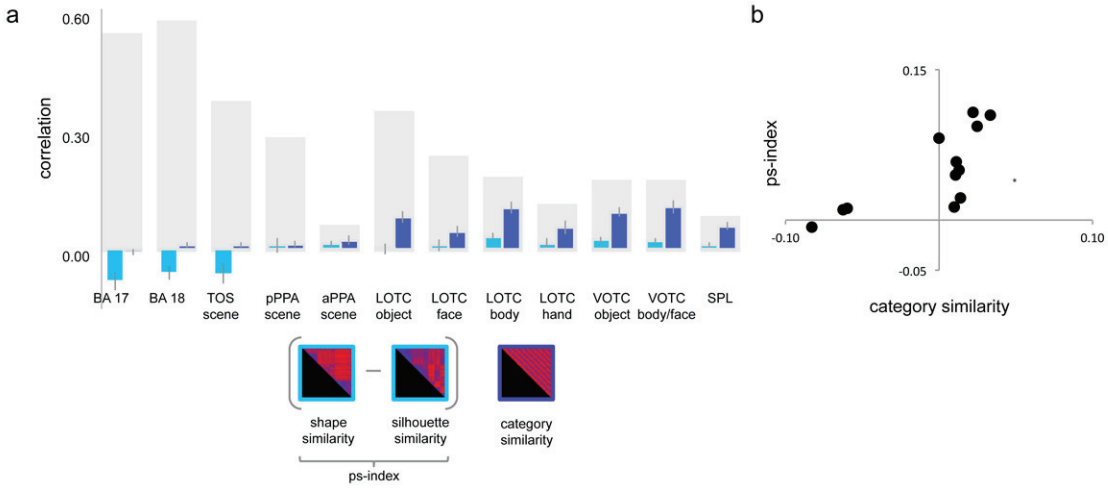

Table 1. ROIs localization. For each ROI, functional contrast, anatomical mask (if used), number of subjects in which the ROI was localized, single subject average MNI coordinates and cluster size are reported.

Author Contributions

S.B. and H.O. designed research; S.B. performed research; S.B. analyzed data;
S.B. and H.O. wrote the paper.

Acknowledgments

This work was supported by the European Research Council (ERC-2011-Stg-284101), a federal research action (IUAP-P7/11), and Hercules grant ZW11_10. We thank Nicky Daniels and Jessica Bulthé for technical assistance. We thank Niko Kriegeskorte for providing the multiple object arrangement code.

References

Arcaro MJ, McMains SA, Singer BD, Kastner S (2009) Retinotopic organization of human ventral visual cortex. The Journal of neuroscience : the official journal of the Society for Neuroscience 29:10638-10652.

Baldassi C, Alemi-Neissi A, Pagan M, Dicarlo JJ, Zecchina R, Zoccolan D (2013) Shape similarity, better than semantic membership, accounts for the structure of visual object representations in a population of monkey inferotemporal neurons. PLoS Comput Biol 9:e1003167.

Bell AH, Hadj-Bouziane F, Frihauf JB, Tootell RB, Ungerleider LG (2009) Object representations in the temporal cortex of monkeys and humans as revealed by functional magnetic resonance imaging. Journal of neurophysiology 101:688-700.

Biederman I (1987) Recognition-by-components: a theory of human image understanding. Psychol Rev 94:115-147.

Bracci S, Ietswaart M, Peelen MV, Cavina-Pratesi C (2010) Dissociable neural responses to hands and non-hand body parts in human left extrastriate visual cortex. J Neurophysiol 103:3389-3397.

Brainard DH (1997) The Psychophysics Toolbox. Spat Vis 10:433-436.

Brincat SL, Connor CE (2004) Underlying principles of visual shape selectivity in posterior inferotemporal cortex. Nature neuroscience 7:880-886.

Buxbaum LJ, Shapiro AD, Coslett HB (2014) Critical brain regions for tool-related and imitative actions: a componential analysis. Brain 137:1971-1985.

Caramazza A, Shelton JR (1998) Domain-specific knowledge systems in the brain the animate-inanimate distinction. Journal of Cognitive Neuroscience 10:1-34.

Chao LL, Martin A (2000) Representation of manipulable man-made objects in the dorsal stream. Neuroimage 12:478-484.

Downing PE, Jiang Y, Shuman M, Kanwisher N (2001) A cortical area selective for visual processing of the human body. Science 293:2470-2473.

Eger E, Ashburner J, Haynes JD, Dolan RJ, Rees G (2008) fMRI activity patterns in human LOC carry information about object exemplars within category. Journal of Cognitive Neuroscience 20:356-370.

Goodale MA, Milner AD (1992) Separate visual pathways for perception and action. Trends Neurosci 15:20-25.

Grill-Spector K, Malach R (2004) The human visual cortex. Annu Rev Neurosci 27:649-677.

Grill-Spector K, Weiner KS (2014) The functional architecture of the ventral temporal cortex and its role in categorization. Nature reviews Neuroscience 15:536-548.

Grill-Spector K, Kushnir T, Hendler T, Edelman S, Itzchak Y, Malach R (1998) A sequence of object-processing stages revealed by fMRI in the human occipital lobe. Human brain mapping 6:316-328.

Grill-Spector K, Kushnir T, Edelman S, Avidan G, Itzchak Y, Malach R (1999) Differential processing of objects under various viewing conditions in the human lateral occipital complex. Neuron 24:187-203.

Hasson U, Levy I, Behrmann M, Hendler T, Malach R (2002) Eccentricity bias as an organizing principle for human high-order object areas. Neuron 34:479-490.

Haushofer J, Livingstone MS, Kanwisher N (2008) Multivariate patterns in object-selective cortex dissociate perceptual and physical shape similarity. PLoS Biol 6:e187.

Haxby JV, Gobbini MI, Furey ML, Ishai A, Schouten JL, Pietrini P (2001) Distributed and overlapping representations of faces and objects in ventral temporal cortex. Science 293:2425-2430.

Hubel DH (1963) The Visual Cortex of the Brain. Sci Am 209:54-62.

Ishai A, Ungerleider LG, Martin A, Schouten JL, Haxby JV (1999) Distributed representation of objects in the human ventral visual pathway. Proceedings of the National Academy of Sciences of the United States of America 96:9379-9384.

James TW, Humphrey GK, Gati JS, Menon RS, Goodale MA (2002) Differential effects of viewpoint on object-driven activation in dorsal and ventral streams. Neuron 35:793-801.

Kanwisher N (2010) Functional specificity in the human brain: a window into the functional architecture of the mind. Proceedings of the National Academy of Sciences of the United States of America 107:11163-11170.

Kayaert G, Biederman I, Vogels R (2003) Shape tuning in macaque inferior temporal cortex. The Journal of neuroscience : the official journal of the Society for Neuroscience 23:3016-3027.

Kiani R, Esteky H, Mirpour K, Tanaka K (2007) Object category structure in response patterns of neuronal population in monkey inferior temporal cortex. Journal of neurophysiology 97:4296-4309.

Kobatake E, Tanaka K (1994) Neuronal selectivities to complex object features in the ventral visual pathway of the macaque cerebral cortex. Journal of neurophysiology 71:856-867.

Konen CS, Kastner S (2008) Two hierarchically organized neural systems for object information in human visual cortex. Nature neuroscience 11:224-231.

Konkle T, Caramazza A (2013) Tripartite organization of the ventral stream by animacy and object size. The Journal of Neuroscience 33:10235-10242.

Kravitz DJ, Saleem KS, Baker CI, Ungerleider LG, Mishkin M (2013) The ventral visual pathway: an expanded neural framework for the processing of object quality. Trends in cognitive sciences 17:26-49.

Kriegeskorte N, Mur M (2012) Inverse MDS: Inferring Dissimilarity Structure from Multiple Item Arrangements. Front Psychol 3:245.

Kriegeskorte N, Mur M, Bandettini P (2008a) Representational similarity analysis - connecting the branches of systems neuroscience. Front Syst Neurosci 2:4.

Kriegeskorte N, Mur M, Ruff DA, Kiani R, Bodurka J, Esteky H, Tanaka K, Bandettini PA (2008b) Matching categorical object representations in inferior temporal cortex of man and monkey. Neuron 60:1126-1141.

Levy I, Hasson U, Avidan G, Hendler T, Malach R (2001) Center-periphery organization of human object areas. Nature neuroscience 4:533-539.

Nasr S, Echavarria CE, Tootell RB (2014) Thinking outside the box: rectilinear shapes selectively activate scene-selective cortex. The Journal of neuroscience : the official journal of the Society for Neuroscience 34:6721-6735.

Nasr S, Liu N, Devaney KJ, Yue X, Rajimehr R, Ungerleider LG, Tootell RB (2011) Scene-selective cortical regions in human and nonhuman primates. The Journal of neuroscience : the official journal of the Society for Neuroscience 31:13771-13785.

Op de Beeck HP (2010) Against hyperacuity in brain reading: spatial smoothing does not hurt multivariate fMRI analyses? Neuroimage 49:1943-1948.

Op de Beeck HP, Haushofer J, Kanwisher NG (2008a) Interpreting fMRI data: maps, modules and dimensions. Nature reviews Neuroscience 9:123-135.
Op de Beeck HP, Torfs K, Wagemans J (2008b) Perceived shape similarity among unfamiliar objects and the organization of the human object vision pathway. J Neurosci 28:10111-10123.
Peelen MV, Downing PE (2005) Selectivity for the human body in the fusiform gyrus. J Neurophysiol 93:603-608.
Puce A, Allison T, Asgari M, Gore JC, McCarthy G (1996) Differential sensitivity of human visual cortex to faces, letterstrings, and textures: a functional magnetic resonance imaging study. J Neurosci 16:5205-5215.
Rajimehr R, Devaney KJ, Bilenko NY, Young JC, Tootell RB (2011) The "parahippocampal place area" responds preferentially to high spatial frequencies in humans and monkeys. PLoS Biol 9:e1000608.
Rice GE, Watson DM, Hartley T, Andrews TJ (2014) Low-level image properties of visual objects predict patterns of neural response across category-selective regions of the ventral visual pathway. The Journal of neuroscience : the official journal of the Society for Neuroscience 34:8837-8844.
Sakuraba S, Sakai S, Yamanaka M, Yokosawa K, Hirayama K (2012) Does the human dorsal stream really process a category for tools? The Journal of neuroscience : the official journal of the Society for Neuroscience 32:3949-3953.
Schwarzlose RF, Baker CI, Kanwisher N (2005) Separate face and body selectivity on the fusiform gyrus. J Neurosci 25:11055-11059.
Valyear KF, Cavina-Pratesi C, Stiglick AJ, Culham JC (2007) Does tool-related fMRI activity within the intraparietal sulcus reflect the plan to grasp? Neuroimage 36 Suppl 2:T94-T108.
Van Essen DC (2005) A Population-Average, Landmark- and Surface-based (PALS) atlas of human cerebral cortex. Neuroimage 28:635-662.
Watson DM, Hartley T, Andrews TJ (2014) Patterns of response to visual scenes are linked to the low-level properties of the image. Neuroimage 99:402-410.
Yamane Y, Carlson ET, Bowman KC, Wang Z, Connor CE (2008) A neural code for three-dimensional object shape in macaque inferotemporal cortex. Nature neuroscience 11:1352-1360.
Yue X, Pourladian IS, Tootell RB, Ungerleider LG (2014) Curvature-processing network in macaque visual cortex. Proceedings of the National Academy of Sciences of the United States of America 111:E3467-3475.